Preprint
UCRL-JC-152243

Effects of Ion Trapping on Crossed-Laser-Beam Stimulated Brillouin Scattering

E.A. Williams, B.I. Cohen, L. Divol, M.R. Dorr, J.A. Hittinger, D.E. Hinkel, A.B. Langdon, R. K. Kirkwood, D.H. Froula and S.H. Glenzer

This article was submitted to Physics of Plasmas

April 18, 2003

DISCLAIMER

Effects of Ion Trapping on Crossed-Laser-Beam Stimulated Brillouin Scattering

E. A. Williams, B. I. Cohen, L. Divol, M. R. Dorr, J. A. Hittinger,
D. E. Hinkel, A. B. Langdon, R. K. Kirkwood, D. H. Froula, and S. H. Glenzer
Lawrence Livermore National Laboratory,
University of California
Livermore, California 94550
(Dated: April 7, 2003)

An analysis of the effects of ion trapping on ion acoustic waves excited by the stimulated Brillouin scattering of crossing intense laser beams is presented. Ion trapping alters the dispersion of ion acoustic waves by nonlinearly shifting the normal mode frequency and by reducing the ion Landau damping. This in turn can influence the energy transfer between two crossing laser beams in the presence of plasma flows such that stimulated Brillouin scattering (SBS) occurs. The same ion trapping physics can influence the saturation of SBS in other circumstances. A one-dimensional analytical model is presented along with reasonably successful comparisons of the theory to results from particle simulations and laboratory experiments. An analysis of the vulnerability of the National Ignition Facility Inertial Confinement Fusion point design is also presented.

PACS numbers: 52.40.Nk, 52.35Mw, 52.65.Rr

I. INTRODUCTION

Nonlinear laser-plasma interactions involving the scattering of intense lasers by collective modes in a plasma have been important in inertial confinement fusion for many years. In many current laser-plasma experimental facilities, multiple intense laser beams interact with target plasmas in which there can be hydrodynamic flows. If two laser beams, the "pump" and the "probe" at frequencies ω_0 and ω_1 respectively, cross at a finite angle in the presence of a flow $\boldsymbol{V}$ such that the following resonance condition is satisfied, then energy transfer from pump to probe by stimulated Brillouin scattering can occur:

$$\omega_0 - \omega_1 = (\boldsymbol{k_0} - \boldsymbol{k_1}) \cdot \boldsymbol{V} + |\boldsymbol{k_0} - \boldsymbol{k_1}| c_s \qquad (1)$$

where $\boldsymbol{k_{0,1}}$ are the wavenumbers of the two crossing laser beams and c_s is the ion sound speed appropriately defined for the particular plasma. In a single ion species plasma, with $ZT_\mathrm{e} \gg T_\mathrm{i}$, $c_\mathrm{s} = (ZT_\mathrm{e}/m_\mathrm{i})^{1/2}$ where $T_\mathrm{e,i}$ are the electron and ion temperatures, Z is the ion charge state, and m_i is the ion mass. We will restrict ourselves, without loss of generality, to the important case where the two lasers have the same frequency, where the condition (1) for energy transfer from pump to probe becomes:

$$(\boldsymbol{k_0} - \boldsymbol{k_1}) \cdot \boldsymbol{V} + |\boldsymbol{k_0} - \boldsymbol{k_1}| c_s = 0 \qquad (2)$$

We note that in order to satisfy the resonance condition in Eq. (2), we must have $|\mathbf{V}| \geq c_s$, such that the component of the flow velocity $\mathbf{V}$ in the direction of transfer, $\boldsymbol{k_1} - \boldsymbol{k_0}$, is equal to the sound speed. Viewed in the moving frame of the plasma flow, the two crossing laser beams have unequal Doppler-shifted frequencies; and if the ponderomotive beat wave frequency and wavenumber of the two lasers resonate with the local ion acoustic wave dispersion relation, the stimulated Brillouin scattering interaction will transfer energy from the higher frequency to the lower frequency laser beam. [1–7]

Current designs for inertial confinement fusion experiments on the National Ignition Facility (NIF) [8] have multiple laser beams crossing as they enter a cylindrical radiation enclosure ("hohlraum"). A finite transfer of energy between the crossing beams can spoil the high degree of illumination symmetry required for the fusion experiments in NIF. [2, 9] Thus, it is important to understand the plasma physics affecting energy transfer between crossing beams in flowing plasmas. Furthermore, the physics of this interaction is relevant to the nonlinear saturation of stimulated Brillouin scattering (SBS) in some circumstances, as has been demonstrated in recent experiments at the TRIDENT facility. [10–14] The saturation of ion acoustic waves in laser plasma interaction experiments is of general interest. [13]

In this paper we present a model for the influence of ion trapping in ion acoustic waves resonantly excited by the ponderomotive force of two nearly parallel, crossing laser beams in a flowing plasma. With the use of a one-dimensional analytical model, we incorporate the effects of ion trapping producing an amplitude-dependent frequency shift in the ion acoustic wave and a reduced level of ion Landau damping into the coupled mode equations for SBS in a flowing plasma. We obtain an analytical solution for the steady-state amplification of the "probe" laser beam (lower frequency laser in the moving frame of the plasma flow) due to its SBS interaction with the "pump" laser (higher frequency laser in the moving frame) in the limit of negligible pump depletion and convection of the driven ion wave. Inclusion of pump depletion leads to a single first-order, nonlinear ordinary differential equation in the one spatial dimension. We present solutions for the probe amplification and the driven ion acoustic wave amplitude with and without pump depletion, and with an imposed frequency mismatch which can represent the influence of having a slightly off-resonant flow velocity. In the limit that there is a gradient in the flow velocity that is oppositely

directed to the direction of the amplifying probe propagation, the nonlinear frequency shift in the ion wave can influence the SBS three-wave matching condition in such a way as to produce "auto-resonance". A bifurcation arises in the nonlinear solution of the driven ion acoustic wave amplitude that is resolved with a boundary layer analysis in which convection of the ion wave is included in the boundary layer. We apply our analysis of ion trapping effects on SBS-resonant crossed-beam interactions to BZOHAR simulations [5, 15] of experiments on the NOVA laser facility published previously. [4, 6] We also review applications of this analysis of ion trapping effects to results from crossing beam experiments in the OMEGA facility at the University of Rochester, [7] to SBS experimental data obtained on TRIDENT at Los Alamos, [10–12, 14] and to a NIF experimental scenario.

A principal conclusion of this paper is that ion trapping provides a potent mechanism for detuning and saturating crossed-beam SBS. The analysis of the simple one-dimensional model presented has some subtlety (bifurcations, auto-resonance, and boundary layer analysis), and the calculations presented provide valuable estimates for use in understanding simulations and experimental results. To be sure, multi-dimensional calculations of crossing-beam phenomena are needed. However, it is useful to have the one-dimensional model as a standard for comparison. Later in the paper we remark on how two-dimensional effects may influence the ion trapping physics and the crossed-beam interaction.

The outline for this paper is as follows. In Sec. I we present an introduction and motivation for the calculations. In Sec. II we give a brief overview of the modifications to the frequency and Landau damping of an ion acoustic wave at finite amplitude when there is ion trapping. We also show how an ion velocity distribution that has been flattened over a trapping width in velocity space can support small-amplitude waves with frequency and damping characteristics approaching those of a finite-amplitude wave with trapping. This quasi-linear treatment of ion waves in a modified ion distribution is used to show the effects of ion wave frequency detuning and dissipation reduction on SBS when the flattening of the ion velocity distribution persists after the primary SBS ion wave has relaxed in amplitude. In Sec. III we present the formalism for a simple one-dimensional model of the influence of ion trapping on crossed-beam SBS in a flowing plasma and exhibit explicit solutions for the steady-state energy transfer between the two laser beams and the concomitant saturated ion wave amplitudes. The effects of pump depletion and flow gradients (parallel and perpendicular to the principal laser propagation direction) are examined. In Sec. IV we discuss the application of our ion trapping model to crossed-beam SBS particle simulations and related experiments on TRIDENT and OMEGA. Our calculations of crossed-beam energy transfer in NIF include multidimensional beam geometry and evolving plasma effects. For the specific NIF inertial confinement fusion (ICF) scenario investigated, the transfer process is found to be non-resonant and ion wave nonlinearities are weak. In an Appendix we present a calculation of the transfer of momentum to the plasma that accompanies crossed-beam energy transfer. Section V concludes the paper with a summary and discussion.

II. ION TRAPPING EFFECTS ON ION WAVES

When the thermal motion of a charged particle is such that its velocity is close to the phase velocity of a traveling longitudinal wave, then in the wave frame the particle can be trapped in the wave trough and its longitudinal excursion is limited because it has insufficient kinetic energy in the wave frame. The trapping of ions and electrons in longitudinal waves has been studied for many years,[16–21] and the influence of trapping on longitudinal waves that are involved in laser plasma interactions has been of great interest. [22–28]

When a longitudinal wave has finite amplitude, the electric field at the particle position is influenced by the finite oscillatory displacement of the particles. An elementary analysis of the nonlinear fluid response of the plasma to a wave leads to the result that there are harmonic generation and quasi-linear effects that produce modifications to the dispersion relation at second order in the wave amplitude [16, 26, 29]. However, the kinetic nonlinearity produced by trapped particles produces a nonlinear modification to the dispersion relation for longitudinal waves that scales with the trapping velocity $v_{\rm t} = (q_{\rm s}\phi/m_{\rm s})^{1/2}$ for small amplitudes. [17–19, 21, 26] (The trapping velocity, $v_{\rm t}$, is the largest characteristic velocity in the wave frame of a particle that can be barely trapped by the longitudinal wave.) Because of its square root scaling, the trapped-particle nonlinearity is dominant at small amplitudes over nonlinearities that scale quadratically. The ion-trapping effects in an ion acoustic wave are quite analogous to the electron-trapping effects in an electron plasma wave. [21] In the absence of collisions, the Landau damping of the resonant particles vanishes after just a few bounce times of the deeply trapped resonant particles. [18] In the presence of weak collisions, the Landau damping remains finite but is reduced by the ratio of the the collision frequency to the trapping frequency. [17] Rose and Russell [28] have extended the Morales and O'Neil[19] calculation to the case of a driven longitudinal wave and obtained a similar result for the frequency shift due to the trapping of a single species (for small frequency shifts such that a perturbation theory is valid).

The expression for the nonlinear frequency shift due to trapping is[19]

$$\frac{\delta\Omega}{\omega} = -\frac{\alpha}{\overline{\epsilon}} v_{\rm t} \Big(\frac{\omega_{\rm ps}}{k}\Big)^2 \frac{\partial^2 f_0}{\partial v^2}, \tag{3}$$

where $\alpha = O(1)$ (Morales and O'Neil calculated $\alpha = 1.63$), $v_{\rm t} = |q_{\rm s}\phi/m_{\rm s}|^{1/2}$ is the trapping velocity for species s (charge $q_{\rm s}$, mass $m_{\rm s}$, plasma frequency $\omega_{\rm ps}$) $\overline{\epsilon} =$

$\omega\partial\epsilon(\omega,k)/\partial\omega$, $\epsilon(\omega,k)$ is the linear longitudinal dielectric function which has been expanded perturbatively around $\epsilon = 0$, and f_0 is the normalized one-dimensional velocity distribution function for the species that can trap in the longitudinal wave. Equation (3) is readily extended to a multiple ion-species plasma. [10] (See Eq. (17).) The formal condition for the validity of the perturbation expansion used in Morales and O'Neil's derivation of Eq. (3) is $v_{\rm t}(\omega/k)/v_{th}^2 << 1$, where $v_{th} = (T_{\rm s}/m_{\rm s})^{1/2}$ is the thermal speed of the species that traps. For ion acoustic waves in a single ion-species plasma the condition that there are some ions that can be trapped is approximately $ZT_{\rm e}/T_{\rm i} < 20$, where Z is the ion charge state, $T_{\rm e}$ is the electron temperature, and $T_{\rm i}$ is the ion temperature.

One-dimensional particle simulations[5, 20] of ponderomotively driven, monochromatic electron plasma and ion acoustic plane waves have yielded results in relatively good agreement with the nonlinear frequency shift in Eq. (3) over more than an order of magnitude in longitudinal wave amplitude, which results extend beyond the validity condition of the Morales and O'Neil perturbation theory. [19] These simulations were dominated by particle trapping, and the velocity distribution functions were flattened in the vicinity of the driven wave phase velocity.

In a collisionless plasma, resonant ions in an ion acoustic travelling wave (or resonant electrons in an electron plasma travelling wave) can trap and flatten their respective velocity distribution functions over a trapping width $v_{\rm t}$ and relax the Landau damping to zero in a few bounce periods of the deeply trapped particles. Both the resonant particle trajectories and the distribution functions are self-consistently modified by the finite-amplitude wave. In the analysis leading to the result in Eq. (3), the wave amplitude is assumed constant. However, in physical situations where the wave amplitude is time dependent and can relax to zero non-adiabatically (compared to the trapped-particle bounce period), the trapped-particle flattened velocity distribution can persist on a long time scale in the absence of the wave that produced the trapping. Such a situation is sometimes realized in stimulated Brillouin and Raman backscattering wherein the principal ion acoustic and electron plasma waves are observed to have a strong bursty time dependence in particle simulations. [5, 15, 22, 24, 27] One mechanism for rapid collapse of high large amplitude ion waves observed in PIC simulations is the two-ion-wave decay instability. [5, 15] In laser-plasma-interaction experiments where trapping can occur, we expect that the modified velocity distribution functions persist until collisions (classical or turbulent) or thermal motion across the laser beams restore the flattened distribution function to a Maxwellian.

In the absence of finite-amplitude waves, a flattened distribution function will give rise to reduced Landau damping and to a frequency shift compared to the resulting dispersion for a Maxwellian, which can be much like that of Eq. (3). Consider the following model distribution function:

$$f(v) = f_M(v) + \beta f_1(v - v_{\rm r}) + \gamma f_2(v - v_{\rm r}), \quad (4a)$$

$$f_1(w) = w\exp(-w^2/2\delta^2), \quad (4b)$$

$$f_2(w) = (\delta^2/3)(w^2/\delta^2 - 1)\exp(-w^2/2\delta^2) \quad (4c)$$

where f_M is a Maxwellian, $v_{\rm r} = \omega/k$ is a resonant velocity chosen to match the phase velocity of a longitudinal test wave, β and γ are constants; and f_1 and f_2 conserve particles, are localized with a width of δ around v_r, and modify the slope and second derivative of f at $v_{\rm r}$, repectively. The standard linear Vlasov calculation of the dispersion relation for a small-amplitude longitudinal wave shows that f_1 affects the Landau damping (for $\beta > 0$ the slope at $v = v_{\rm r}$ and the Landau damping are reduced), while f_2 induces a frequency shift:

$$\frac{\delta\omega}{\omega} = \frac{2\sqrt{2\pi}}{3\overline{\epsilon}_M}\frac{\omega_{\rm ps}^2}{k^2}\gamma\delta \quad (5)$$

where $\overline{\epsilon}_M = \omega\partial\epsilon_{\rm M}/\partial\omega$ and $\omega_{\rm ps}$ is the plasma frequency of the resonant species s. If we set $\delta = v_{\rm t}$ (the trapping width of the finite-amplitude wave responsible for the flattening) and $\gamma = -\partial^2 f_M/\partial v^2$ at $v = v_{\rm r} = \omega/k$, then from Eq. (5),

$$\delta\omega/\omega = -0.83 v_{\rm t} v_{\rm r}^2 d^2 f_M/dv^2|_{v=v_{\rm r}}, \quad (6)$$

which agrees with the result of Morales and O'Neil[19] to within 2% except that this frequency shift is for a linear test wave. β can be independently chosen so that $\partial f/\partial v = 0$ at $v = v_{\rm r}$ and $f(v)$ supports no Landau damping. This calculation is in the spirit of a quasi-linear calculation of the linear dispersion relation for a test wave as influenced by a flattened velocity distribution.

The results of this section and prior publications demonstrate that trapping produces a negative frequency shift and reduces the Landau damping for a resonant electron plasma wave or an ion acoustic wave with or without the simultaneous presence of a large-amplitude wave. In the next section we incorporate the frequency detuning effects of ion trapping into a model for the nonlinear saturation of the stimulated Brillouin interaction of crossed laser beams in a flowing plasma.

III. STIMULATED BRILLOUIN INTERACTION AND ION TRAPPING

A. Stimulated Brillouin scattering coupled-mode equations with ion trapping detuning

We consider the following steady-state coupled-mode equations for stimulated Brillouin scattering in one spa-

tial dimension: [30, 31]

$$v_g da_0/dx = -\Gamma a_1 a_s \quad (7a)$$

$$\pm v_g da_1/dx = \Gamma a_0 a_s^* \quad (7b)$$

$$\left(v_s \frac{d}{dx} + \nu + i(\Delta_0 - \eta\omega_s |a_s|^{1/2})\right) a_s = \Gamma a_0 a_1^* \quad (7c)$$

where a_0 and a_1 are the electromagnetic wave amplitudes of the "pump" and "probe" waves (e.g., higher and lower-frequency crossing laser beams in the flowing plasma frame), $a_s = \delta n_e/n_e$ is the relative electron density perturbation in the ion wave, the $\pm$ in Eq. (7b) corresponds to forward and backward scattering, respectively, v_g is the group velocity of the electromagnetic waves (taken equal here because $\omega_s \ll \omega_0, \omega_1$), η is related to the numerical factor determined by Eq. (3) or (6), ν is the ion wave dissipation rate, v_s is the group velocity of the sound wave ($v_s \approx c_s$), Δ_0 is a constant frequency mismatch factor, $\Gamma^2|a_0|^2 = (\omega_s/\omega_0)\omega_{pe}^2(v_0^2/16v_e^2)$ is the square of the SBS homogeneous-medium growth rate, $v_e^2 = T_e/m_e$, and $v_0 = eE_0/m_e\omega_0$ is the transverse electron quiver velocity in the pump wave. We can assign values to Δ_0 to accommodate the effects of a gradient in the flow that is perpendicular to the laser-beam propagation direction.

In the limits that $|a_1| << |a_0|$ and ion wave convection in Eq. (7c) is negligible compared to the dissipation and mismatch terms, Eqs. (7b) and (7c) can be solved analytically. We use Eq. (7c) to solve for a_1 in terms of a_s, introduce $a_s = r^2 e^{i\theta}$, use real and imaginary parts of Eq. (7b) to determine $d\theta/dx$ in terms of dr/dx, and obtain

$$\frac{d\ln r^2}{dx} + \frac{1}{\overline{\nu}^2}(3\eta^2 r - 5\eta\overline{\Delta} + \frac{2\overline{\Delta}^2}{r})\frac{dr}{dx} = \kappa, \quad (8)$$

where $\overline{\nu} = \nu/\omega_s$, $\overline{\Delta} = \Delta_0/\omega_s$, and the linear spatial gain rate for the probe amplitude is $\kappa = \Gamma^2/v_g\nu$. We integrate Eq. (8) to obtain

$$\left[(1+\overline{\Delta}^2)\ln r^2 + \frac{3}{2}\frac{\eta^2}{\overline{\nu}^2}r^2 - \frac{5\eta\overline{\Delta}}{\overline{\nu}^2}r\right]\Bigg|_{r(0)}^{r(x)} = \kappa x, \quad (9)$$

for near forward scatter ($-\kappa x$ for backward scatter). If the nonlinear frequency shift is a weak effect compared to the dissipation, i.e., $\eta/\overline{\nu} << 1$, the probe beam amplifies exponentially in space with rate $\kappa/(1+\overline{\Delta}^2)$. For the detuning due to ion trapping to be significant, $\eta/\overline{\nu} \geq O(1)$. For $\eta/\overline{\nu} >> 1$, the ion wave and probe beam amplitudes grow algebraically in space.

B. Pump depletion effects

To include pump depletion, we relax the assumption that $|a_1| << |a_0|$ and retain Eq. (7a). Equations (7a) and (7b) admit the conservation law,

$$v_g \frac{d}{dx}\left(|a_0|^2 \pm |a_1|^2\right) = 0, \quad (10)$$

for forward and backward scatter, respectively. Hence, $|a_0|^2 \pm |a_1|^2 = |a_0(0)|^2 \pm |a_1(0)|^2 = P \pm S$, where P and S are the pump and probe (i.e., scattered) beam intensity boundary conditions at $x = 0$. It then follows that $|a_0|^2 = P \pm S \mp |a_1|^2$ for forward and backward scattering, respectively. From Eqs.(7b) and (7c) we then obtain

$$\pm v_g \frac{d}{dx}|a_1|^2 = 2\nu|a_s|^2, \quad (11a)$$

$$|a_s|^2(\nu^2 + \Delta^2) = \Gamma^2|a_1|^2(P \pm S \mp |a_1|^2), \quad (11b)$$

for forward and backward scatter, where $\Delta = \Delta_0 - \eta\omega_s|a_s|^{1/2}$. We solve Eqs.(11), in the forward scatter geometry, by solving the second relation algebraically for $|a_s|$ with a convergent iterative solver at each position, substituting the result into the right side of the first relation, and numerically integrating the differential equation for $|a_1|^2$ using a centered, second-order-accurate, predictor-corrector scheme. Examples of the solutions for the probe amplitudes and concomitant electron density perturbations with and without pump depletion will be presented in Sec. IV. Because of the nonlinearities in Eqs.(9) and (11), there are multiple physical solutions and bifurcations possible, which are elucidated in the next subsection and in the examples in Sec. IV.

In the case of a backscatter pump-probe geometry, S is a priori unknown. It is $|a_1|^2(L)$, the probe intensity entering the $x = L$ boundary of the interaction region that is prescribed by the physical boundary conditions. A further iteration is required to choose S to match this condition.

C. Parallel gradients and auto-resonance

We next consider the extension of Eqs.(7b) and (7c) for forward scattering to include a spatial gradient affecting the ion-wave dispersion (e.g., a spatial gradient in the flow) and assume that there is negligible pump depletion (a_0 is a constant):

$$v_g \frac{da_1}{dx} = \gamma_{0s} a_s^*, \quad (12a)$$

$$(v_s \frac{d}{dx} + \nu + i\kappa' v_s(x - x_r) - i\eta\omega_s|a_s|^{\frac{1}{2}})a_s = \gamma_{01} a_1^*, \quad (12b)$$

where $\kappa' v_s = d\Delta\omega_s/dx$, $\Delta\omega_s = |\mathbf{k}_0 - \mathbf{k}_1|c_s - \left[\omega_0 - \omega_1 + (\mathbf{k}_0 - \mathbf{k}_1)\cdot\mathbf{v_d}\right]$, and $\gamma_{01}\gamma_{0s} = \gamma_{sbs}^2$. γ_{sbs} is the homogeneous temporal growth-rate for the SBS process. We next introduce dimensionless units (temporarily suppressing

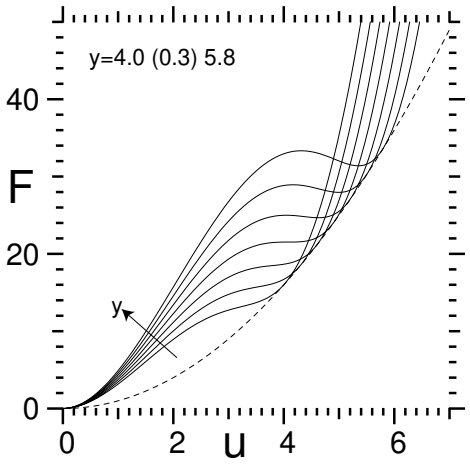

FIG. 1: $F = u^2\big(1+(y-u)^2\big)^{1/2}$, where $u = \eta\omega_s|\delta n_e/n_e|^{1/2}/\nu$ determines the ion wave amplitude for a given ponderomotive force. Multiple roots for $u(F)$ are possible when $y > \sqrt{24}$.

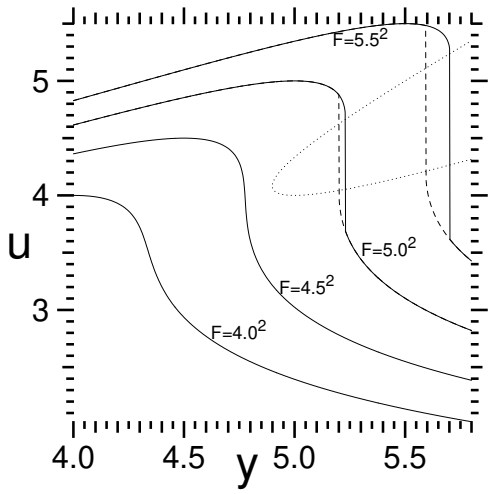

FIG. 2: Solutions of $F = u^2\big(1+(y-u)^2\big)^{1/2}$ for $u = \eta\omega_s|\delta n_e/n_e|^{1/2}/\nu$ as a function of $y = \kappa' v_s(x-x_r)/\nu$ for $F = 4^2, 4.5^2, 5^2, 5.5^2$, where F is proportional to the ponderomotive force. The solid curves are the largest root, the dashed curves the smallest, appropriate for $\kappa' >< 0$, respectively. The dotted curve is the condition for $dF/du = 0$: $u = 5y/6 \pm (y^2-24)^{1/2}/6$.

$v_s da_s/dx$):

$$\frac{dw}{dy} = \frac{2\Lambda}{1+(y-u)^2} \tag{13a}$$

$$u^4(1+(y-u)^2) = 2\hat{\beta}e^w \tag{13b}$$

where $\Lambda = \gamma_{01}\gamma_{0s}/\kappa' v_g v_s$ is the Rosenbluth [32] gain parameter, $w = \ln(|a_1|^2/|a_1(y_0)|^2)$ is the probe intensity gain exponent, $u = \eta\omega_s|a_s|^{1/2}/\nu$ is the ratio of the magnitude of the nonlinear frequency shift to the ion wave damping rate, $y = \kappa' v_s(x-x_r)/\nu$ is the ratio of the inhomogeneity frequency mismatch to the ion wave damping rate (which frequency mismatch increases linearly in magnitude with distance away from the resonance position x_r), and $\hat{\beta} = (1/2)(\gamma_{01}/\nu)^2(\eta\omega_s/\nu)^4|a_1(y_0)|^2$. The point y_0 is an arbitrary reference point; we will take $y_0 = 0$, the linear matching point. u and w are thus measures of the ion wave amplitude and the pump-probe energy transfer, respectively. $\hat{\beta}$ is proportional to the product of the pump and probe intensities and $\hat{\beta} = 1$ implies $u = 1$ at $y = y_0$, that is, the beat ponderomotive force at the reference point is sufficient to drive the ion wave to an amplitude where its nonlinear frequency shift equals its damping rate.

Integration of Eq. (13a) through the resonant region obtains the total exponentiation, $G \equiv w|_{x=-\infty}^{x=\infty}$ of the probe. This requires solving Eq. (13b) for u, given $F^2 \equiv 2\hat{\beta}\exp(w)$. In the linear ion wave limit, where $\eta = \hat{\beta} = 0$, trivially $u = 0$, giving a gain $G = 2\pi|\Lambda|$, the Rosenbluth [32] result. However, for sufficiently large ponderomotive force, $F^2 > 12500/27$, Eq. (13b) has three roots for u over a range of y with $y > \sqrt{24}$. Otherwise the (positive) root is unique. In Fig. 1, we plot $F(u)$ for a series of values of y bracketing $y = \sqrt{24} \simeq 4.9$ where the inflection point first occurs. The dotted envelope curve is the resonant response $F = u^2$.

To remove this ambiguity of the reduced model described by Eqs. (13), we restore the ion wave convective term in Eq. (12b) and consider the singular limit $v_s \to 0$. A perturbation analysis of Eq. (12b) readily shows that whenever the roots of Eq. (13b) are unique they are stable attractors of the ODE (12b). When there are three roots, those with the smallest and largest magnitudes are stable and the intermediate root is unstable. Solutions of the ion wave ODE (12b), with fixed or slowly varying RHS, relax to the stable roots of the algebraic equation on the scale of the ion damping length v_s/ν.

The limiting root varies continuously as y and F change – except that on disappearance of the root (at a point where $\partial F/\partial u = 0$ and $u = 5y/6 \pm (y^2-24)^{1/2}/6$) the solution jumps discontinuously to the remaining root. Retention of the ion wave convective derivative resolves the discontinuity into an internal boundary layer of thickness of order the ion wave damping length. In Fig. 2 we plot the stable root(s) of Eq. (13b) as a function of y for several values of F. The physical root is the larger one when $\kappa' > 0$ and the smaller (shown dashed) when $\kappa' < 0$. In Fig. 3 we integrate Eq. (12b) directly over a narrow range of y for fixed F and various values of v_s decreasing to zero, in the case $\kappa' > 0$ to illustrate how the solution converges towards the discontinuous one described above. Note that condition for the neglect of the ion wave convection is, for the case of backscatter geometry, also that of being below the threshold for absolute instability. Absolute instability would of course make our steady-state treatment inappropriate.

We see from Eq. (13a) that the nonlinear frequency shift moves the effective resonance point to $y > 0$. Indeed, the maximum ion wave response occurs where $y = u = \sqrt{F}$, as can also be seen in Fig. 2. If the ion

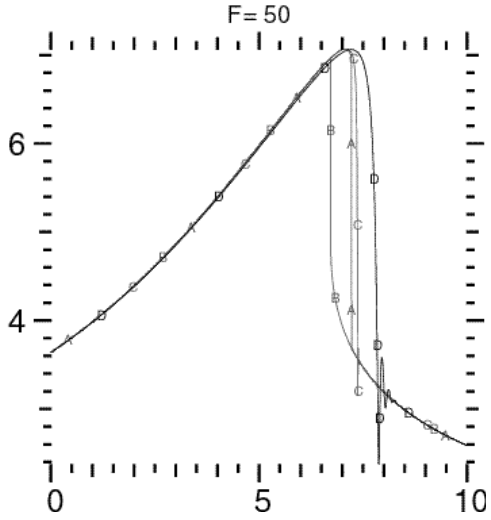

FIG. 3: Curves A and B are the largest and smallest solutions of $F = u^2\left(1+(y-u)^2\right)^{1/2}$ for $F = 50$. Curves D and C are corresponding solutions of Eq. (12b) with decreasing values of v_s – which converge to curve A as v_s vanishes.

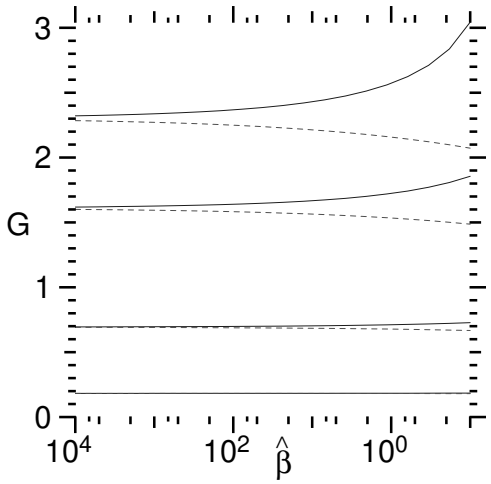

FIG. 4: Total gain $G \equiv w|_{-\infty}^{\infty}$ as a function of $\hat{\beta} \equiv (1/2)(\gamma_{01}/\nu)^2(\eta\omega_s/\nu)^4|a_1(0)|^2$ for linear amplifications $\exp(2\pi\Lambda) = 1.2, 2, 5, 10$. Solid (dashed) curves are the (anti-)autoresonant cases.

wave nonlinear frequency shift is small compared to the damping rate throughout the resonant region ($u \ll 1$), clearly the gain G remains close to the linear Rosenbluth result. The same is true even if the shift is not small provided the gain is small. In this case u is finite but approximately constant through the resonant interaction region.

The more interesting situation, in which the nonlinear frequency shift is effective, is when both the shift and the gain are finite. In this case, the u in the denominator of Eq. (13a) cannot be treated as constant. Here, the sign of κ' is important. The sign of κ' is determined by the direction of the gradient. $\kappa' > 0$ corresponds to increasing sound speed or decreasing flow velocity in the direction of probe amplification. In this case, $\partial u/\partial y > 0$ giving rise to partial cancellation in the $(y-u)^2$ term in the denominator of Eq. (13a), which nonlinearly enhances the magnitude of the probe intensity gain ("auto-resonant"). Conversely, when $\kappa' < 0$, $\partial u/\partial y < 0$ and the increasing trapping nonlinearity enhances the gradient detuning of the resonance ("anti-auto-resonant"). The nonlinear gain in this case is less than the Rosenbluth gain. In Fig. 4, we plot the gain G as a function of the nonlinearity parameter $\hat{\beta}$ for several values of the gain parameter $|\Lambda|$ ($\exp(2\pi|\Lambda|) = [1.2, 2, 5, 10]$). Note that as $\hat{\beta} \to 0$, the gain G goes to the Rosenbluth limit $2\pi|\Lambda|$. As $\hat{\beta}$ increases, the resulting gain increases in the auto-resonant case and decreases when anti-auto-resonant. The effect of ion wave nonlinearity increases with increasing gain.

IV. APPLICATIONS TO PARTICLE SIMULATIONS AND EXPERIMENTS

In this section we apply the foregoing analysis to examples drawn from particle simulations of crossed-beam interactions and to crossed-beam and SBS experiments. We also consider a crossed-beam scenario for parameters proposed for experiments in the National Ignition Facility. Our theory of the SBS interaction including trapped ion effects indicates that trapping can lead to significant detuning of the SBS interaction if the magnitude of the numerical factor η appearing in the nonlinear frequency shift determined in Eq. (3) or (6) is big enough so that the frequency shift term is competitive with the ion wave damping rate. The frequency shift is given by $-\eta\omega_s(\delta n_e/n_e)^{1/2}$. In Fig. 5 we plot the value of η as a function of ZT_e/T_i for a single-ion-species plasma for various values of $k_a\lambda_e$, where k_a is the ion acoustic wavenumber and $\lambda_e = v_e/\omega_{pe}$ is the electron Debye length. We conclude that ion-trapping detuning can affect the resonant SBS interaction for $ZT_e/T_i < 20$, and this is seen in the following examples.

A. Particle simulations of crossed-beam energy transfer

The BZOHAR[16] fluid-particle hybrid simulation code was used to undertake simulations of the resonant SBS interaction of opposed laser beams for experiments in NOVA[6], which was reported in an earlier publication. [5] These simulations were undertaken in a rectangular box ($64\lambda_0$ in x and $4\lambda_0$ in y, where λ_0 is the laser wavelength) with periodic boundary conditions in y and open boundary conditions on the electromagnetic waves in x. A detailed description of the simulations is given in Ref. 5. The simulations exhibited significant periods of high probe amplification (reflectivity) early in the simulations followed by a general reduction in the probe amplification toward a quasi-steady state in which

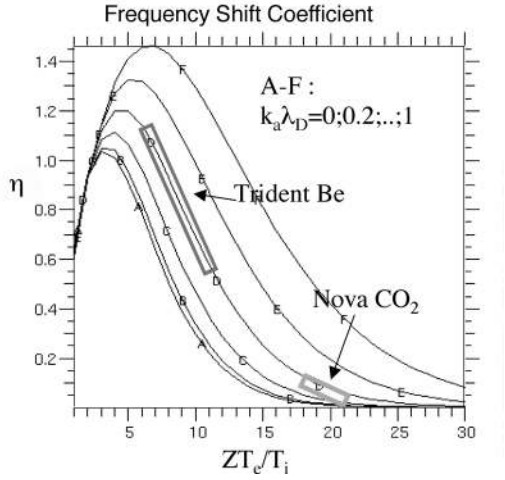

FIG. 5: Nonlinear frequency shift coefficient η vs. $ZT_\mathrm{e}/T_\mathrm{i}$ for various values of $k_a\lambda_e$ determined by Eq. (3).

there was significant trapping, flattening of the longitudinal ion velocity distribution, and hot-ion tail formation. In Fig. 6 we compare theoretical predictions based on Eq. (9) for the intensity amplifications of the backscattered probe beam exiting the plasma $|a_1/a_1(0)|^2$ to those observed at the end of the BZOHAR simulations (40 psec) as a function of the ratio of input intensities of the pump wave to the input intensity of the probe wave ($I^{in}_{pump} = 1.6 \times 10^{15}\mathrm{W/cm^2}$) in a Be plasma with time-averaged ion acoustic damping $\nu/\omega_s = 0.03$, $\eta = 0.4$, $\Delta_0 = 0$, $k_a\lambda_\mathrm{e} = 0.38$, $\lambda_0 = 0.35\mu$m wavelength light, $n_\mathrm{e}/n_c = 0.1$, $v_0/v_\mathrm{e} = 0.2$, $T_\mathrm{e} = 2\mathrm{K}eV$, and $ZT_\mathrm{e}/T_\mathrm{i} = 9.6$ with an effective interaction length $L = 48\lambda_0$ determined by an imposed modulation of the plasma drift velocity. The ion-trapping theory agrees quite well with the simulation data for the parameters used to evaluate the theory.

B. Applications to experiments

The trapping theory derived here was applied to SBS backscatter experiments in the TRIDENT Laser Facility[33] and reported in earlier publications. [10–12] In the TRIDENT SBS experiments, gold and berylium target plasmas were used, and SBS reflectivities, ion wave amplitudes (relative to thermal levels), and ion heating were diagnosed. Based on linear theory for the SBS reflectivities in these experiments, one expects $\sim 100\%$ reflectivities; instead $\sim 10\%$ reflectivities were observed. The Thomson scattering diagnostics show that ion heating correlates with higher ion-acoustic wave amplitudes detected. In Fig. 7 (taken from Ref. 10) are shown the observed SBS reflectivities in TRIDENT as a function of the percent concentration of Au as well as the predictions of Eq. (9) using a residual ion wave damping set by electron Landau damping and collisions $\nu/\omega_s = 0.015$, $L = 800\mu$m, $T_{Be}/T_\mathrm{e} = 1/2$, $I^{in}_{pump} = 3 \times 10^{15}\mathrm{W/cm^2}$, $n_e = 10^{20}\mathrm{cm}^{-3}$. Here n_c is the critical density where the laser frequency equals the local electron plasma frequency. The value of η in Eq. (9) was determined as a function of the Au concentration using Eq. (3) and is shown in Fig. 8 (also taken from Ref. 10). The value of η increases while the phase velocity decreases for increasing Au concentration. To obtain the theoretical values in Fig. 7, the higher value of η corresponding to the higher ion temperature (after the ions have heated due to the trapping) was used. We note that the nonlinear detuning from ion trapping becomes important in this case when $|\delta n/n_\mathrm{e}| \approx \nu^2/\eta^2\omega_s^2 \approx 0.1\%$, i.e., when the nonlinear frequency shift and the ion wave damping are comparable. The spread of theory values in Fig. 7 is due to the uncertainties in the electron density and the interaction beam intensity. For an Au concentration exceeding 10%, inverse bremsstrahlung and collisional ion effects need to be included. The theory captures the trends in the experimental data quite well, and there is semi-quantitative agreement.

We caution that applying our ion-trapping detuning theory to SBS raises some questions. In the crossed-beam interaction, the beat-wave frequency and wavenumber in the flowing plasma are well defined because of the finite amplitudes of the pump and probe waves. For the case of SBS amplification of the probe signal from noise, a finite-frequency-bandwidth noise source is a more appropriate model for the probe boundary condition. SBS amplification over a significant bandwidth might reduce both the ion-trapping effects (by providing a decorrelation mechanism) and the concomitant detuning influence on the SBS. However, even with finite bandwidth and loss of coherent wave-particle trapping, flattening of the ion distribution function over a range of phase velocities can still occur due to wave-particle interaction. Such flattening can result in similar levels of frequency shift in the ion waves and reduction of the linear ion Landau damping as those due to trapping (see Sec. II), in which case the predictions of our trapping theory for the SBS saturation may still be relevant.

Our analysis of the effects of ion trapping on the SBS interaction has also been applied to crossed-beam experiments at the University of Rochester OMEGA laser facility. [7] Here we provide additional calculations. The geometry in the OMEGA experiments corresponds to nearly forward scattering with the plasma density and flow gradients largely perpendicular to the laser propagation direction. In Figs. 9a and 9b we show solutions of Eq. (9) with no pump depletion and Eq. (11) with pump depletion included, respectively, for a scan of pump intensities and with parameters $n_\mathrm{e}/n_\mathrm{c} = 3\%$ and 6.4%, intensity attenuation factors to account for inverse bremsstrahlung equal to 93% and 70% for the low and high-density cases, residual ion wave damping due to electron Landau damping and ion collisions $\nu/\omega_s = 0.015$, $\Delta_{nl}/\omega_s = -0.5|\delta n/n_\mathrm{e}|^{1/2}$, $I^{in}_{probe} = 1.2 \times 10^{14}\mathrm{W/cm^2}$, $\lambda_0 = 0.35\mu$m, $T_\mathrm{e} \approx 1.2\mathrm{K}eV$, and effective length $L = 65\mu$m. In Ref. 7 we presented similar cal-

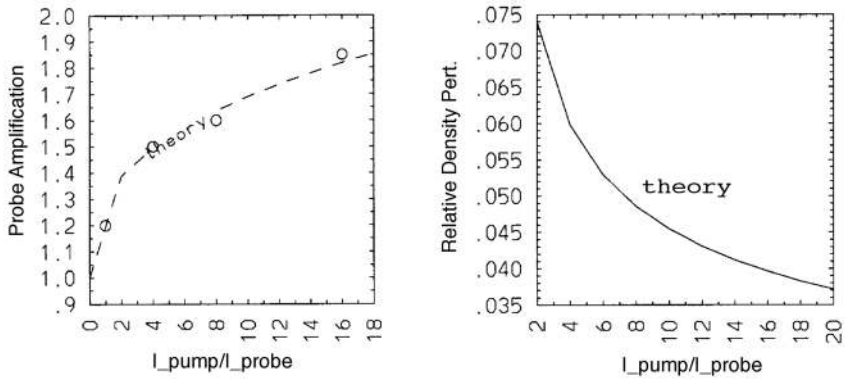

FIG. 6: From BZOHAR hybrid simulations of opposed crossed beams, probe intensity amplifications and maximum relative electron density perturbations in the ion wave vs. input ratio $I^{in}_{pump}/I^{in}_{probe}$.

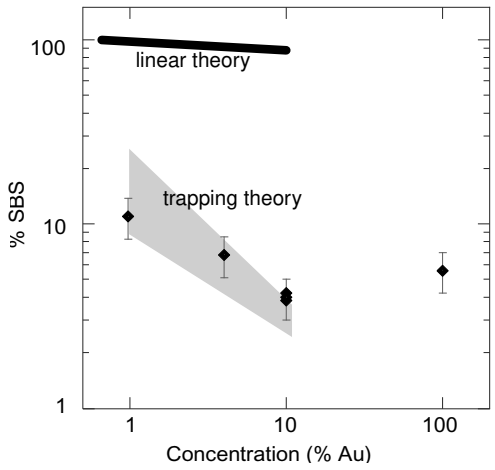

FIG. 7: SBS reflectivity as a function of Au concentration for TRIDENT SBS experiments. The expectation of linear theory is indicated by the black line. The shaded band corresponds to the predictions of Eq. (9) including experimental uncertainties in the parameters.

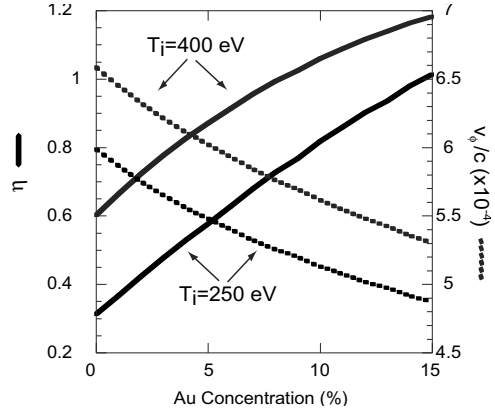

FIG. 8: The nonlinear frequency shift coefficient η and the ion wave phase velocity vs. Au concentration in a Be + Au plasma at ion temperatures before and after ion heating.

culations using $L = 75\mu$m, which we have revised here based on a more recent, improved numerical calculation of the two-dimensional SBS coupled-mode equations taking into account a finite beam-overlap region, the relative aiming of the two laser beams, refraction, the evolving gradients of the expanding plasma, and nonlinear laser-beam bending due to the flow and ponderomotive effects. However, this numerical calculation omits ion wave nonlinearity and pump depletion. The revised effective interaction length $L = 65\mu$m was calculated by equating $e^{\kappa L}$ to the observed beam-averaged amplification of the probe amplitude in the two-dimensional numerical calculation. Including pump depletion in the calculations displayed in Fig. 11 reduced the probe intensity amplification by $< 10\%$ at the highest pump power and by a lesser amount at the lower pump powers. In Figs. 10 and 11 we show the results of solutions for Eq. (9) with no pump depletion and Eq. (11) with pump depletion included, respectively, for a scan of probe intensities with parameters $n_e/n_c = 6.4\%$, $I^{in}_{pump} = 7\times10^{14}$W/cm^2 and other parameters the same as in the pump intensity scan in Figs. 9. Inclusion of pump depletion reduces the probe amplifications by $< 10\%$ in the results shown in Figs. 9b and 11. The decrease in probe amplification with increasing probe intensity is a clear signature of a nonlinear effect (in the absence of nonlinear saturation the probe amplification as a function of probe intensity is a constant). The theoretical results in Figs. 11, 9 and 10 capture the trends of the experimental data quite well. However, these results do not convince us that the ion trapping nonlinearity is the dominant nonlinearity; in these experiments there were measurements of the transmitted beam intensities but no Thomson scattering measurements of concomitant ion wave amplitudes or ion heating, and local pump depletion in intense speckles may have occurred.

To address the influence of a fixed frequency mismatch, for example due to the crossed-beam interaction not occurring at the Mach 1 layer ($v_d = c_s$), we have solved Eq. (9) as a function of the drift speed v_d/c_s that determines the linear mismatch frequency for

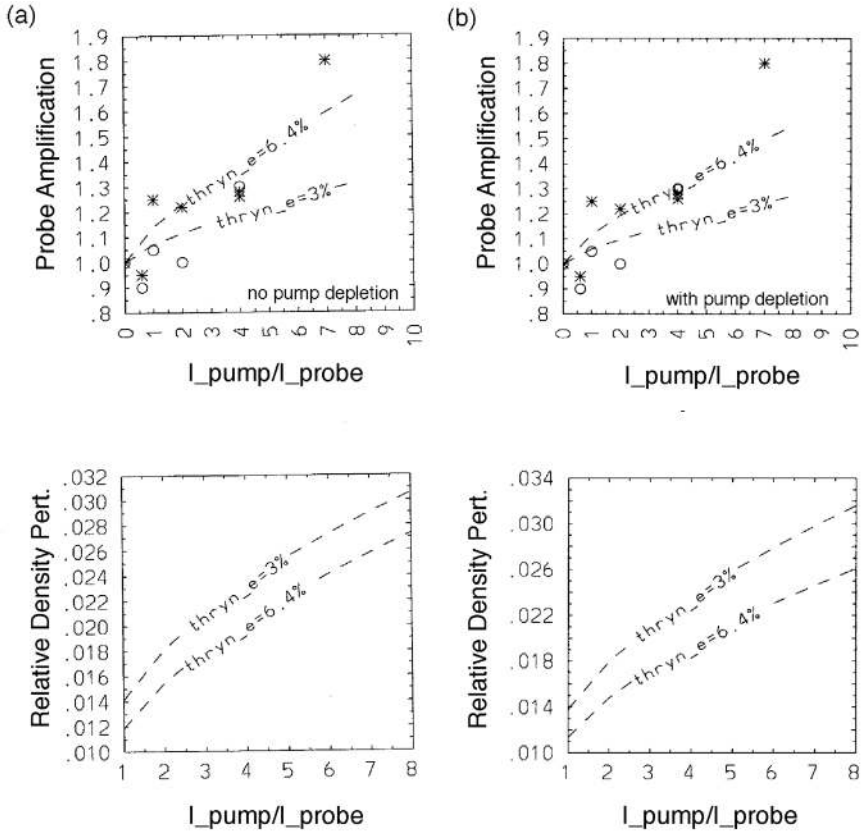

FIG. 9: Theoretical estimates (curves) and OMEGA experimental observations (points) of probe intensity amplifications and maximum ion wave electron density perturbations vs. input ratio $I^{in}_{pump}/I^{in}_{probe}$ for $n_e/n_c = 3\%$ and 6.4%, (a) with no pump depletion and (b) with pump depletion included in the theory.

$I^{in}_{pump} = 7 \times 10^{14}\mathrm{W/cm^2}$, $I^{in}_{probe}/I^{in}_{pump} = 0.17$ and 10^{-6}, $n_e/n_c = 6.4\%$, $L = 65\mu$m, and other parameters the same as for Fig. 9. The gain curve with respect to v_d/c_s in Fig. 12 shows that the peak amplitude is shifted nonlinearly to lower drift velocities (where pump depletion effects should be included for the higher input probe intensity case) because of the auto-resonance effect. The probe amplification as a function of drift speed has a slower variation for $v_d > c_s$, which is related to anti-auto-resonance. The discontinuous behavior observed in the gain curve is directly related to the omission of the ion wave convection discussed in Sec. III. The nonlinear detuning effect in the crossed-beam case broadens the gain curve and shifts it to lower drift speeds. The nonlinear effects are much weaker in the SBS limit considered ($I^{in}_{probe}/I^{in}_{pump} = 10^{-6}$). For the same parameters, we did additional calculations in which the electron density of the freely expanding target plasma was related to the drift velocity of the expanding plasma as described by the simple self-similar solution, $n_e \sim e^{-x/c_s t}$ with $x = vt$ so that $n_e \sim e^{-v/c_s}$. There was very little change in the probe gain and peak electron density curves because these curves peak in a relatively narrow range near the Mach 1 layer.

C. Application to the NIF ICF point design

In the National Ignition Facility there will be multiple crossing laser beams entering the hohlraum through two laser entrance holes (LEH). Plasma created inside the hohlraum will stream out of the LEH supersonically and then fan out radially. Inside the LEH the flow will be subsonic. If the resonance condition in Eq. (2) is satisfied by the crossing beams, then the power distribution between the inner and outer laser beams may be altered, which can then spoil the implosion symmetry of the target capsule. A specific scenario is depicted in Figs. 13 and 14 based on calculation of the hohlraum plasma and laser dynamics performed with the LASNEX [34] two-dimensional and HYDRA [35, 36] laser-fusion simulation codes [37, 38]. We see in Fig. 13 that the most vulnerable time for crossed-beam energy transfer is when the inner beams reach their peak power at 15.2 ns. At this point in time, the NIF laser is at its nominal design power limit and so one could not plan to compensate for power transfer by putting more power into the inner beams. At this time the envelope focal intensity of the inner and outer beams are $1. \times 10^{15}$ and $6.7 \times 10^{14}\mathrm{W/cm^2}$, respectively. There is little absorption or diffractive spreading of the

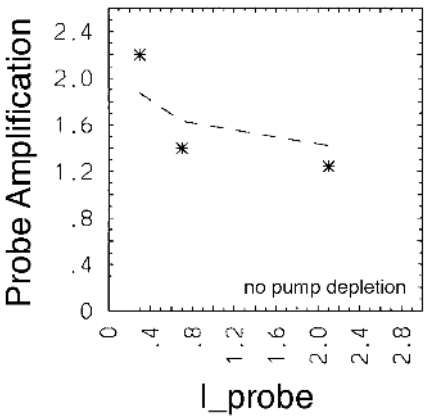

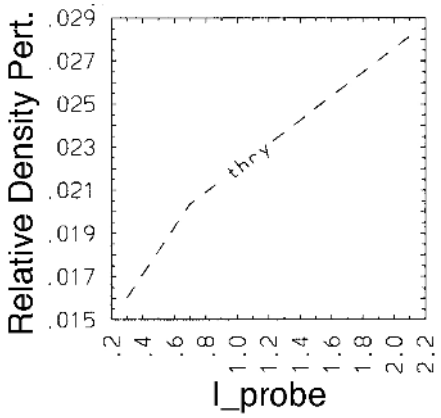

FIG. 10: Theoretical estimates (curves) and OMEGA experimental observations (points) of probe intensity amplifications and maximum ion wave electron density perturbations vs. input probe intensity (in units of 10^{14}W/cm^2) for $n_e/n_c = 6.4\%$ with no pump depletion included in the theory.

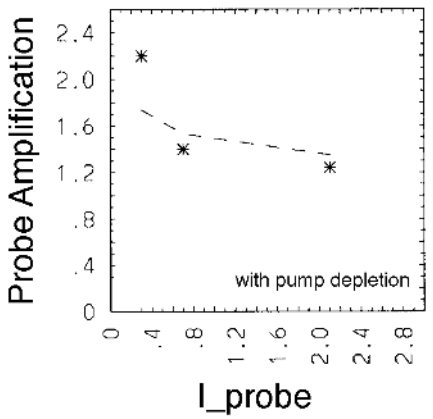

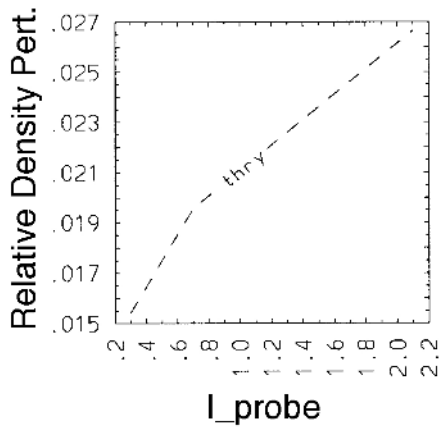

FIG. 11: Theoretical estimates (curves) and OMEGA experimental observations (points) of probe intensity amplifications and maximum ion wave electron density perturbations vs. input probe intensity (in units of 10^{14}W/cm^2) for $n_e/n_c = 6.4\%$ with pump depletion included in the theory.

beams in the crossing region outside the LEH, so these intensities are also representative there. The approximate location of the crossing-beam interaction is depicted in Fig. 14. There are in fact four cones of beams entering each LEH. Eight quads at 50° and at 44.5° to the hohlraum axis are termed the outer beams. Four quads at 30° andat 23° form the inner beams. Each cone of beams is arranged symmetrically around the azimuthal axis. The geometry of the beams, the flow and the resonance condition for crossed beam energy transfer are complicated. The radial fanning of the flow limits where the resonance condition can be satisfied. Indeed we see that in this design, the simulations indicate that the resonance condition is never satisfied inside the crossing volumes despite the flow speed being supersonic throughout.

However, lack of resonance does not mean that power transfer cannot occur, only that it will be significantly reduced. In Fig. 16 we plot the amplitude spatial growth rate, g for the forward SBS responsible for power transfer as a function of transverse velocity for two typical conditions bracketing those in the crossing volume, given by

$$g = \frac{1}{8}\left(\frac{v_0}{c}\right)^2 \frac{k^2}{k_0}\mathrm{Im}(\chi_e(1+\chi_i)/(1+\chi_e+\chi_i) \qquad (14)$$

Except for a narrow jet of H/He plasma on the hohlraum axis about 400μm in diameter, the crossing volume is filled with fully ionized CH ablated from a coating on the LEH. The curves in Fig. 16 is computed using electron and ion susceptibilities $\chi_{ei}(-kV, k)$ for this material. At the Mach 1 resonance, we see that amplitude spatial growth rates range from 8-12 cm^{-1}. However, the peak transverse velocities in the crossing region are only 2-3$\times 10^7$ cm/sec, reducing the growth rates by an order of magnitude.

To quantify the expected beam to beam transfer, for each inner/outer beam pair, the gain coefficient g (in Eq. (14)) was integrated along the inner beam path through the region of intersection with the outer beam. This

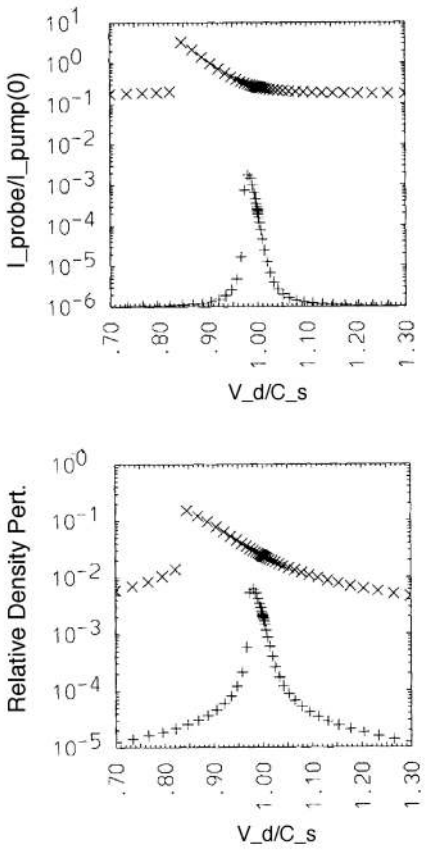

FIG. 12: Theoretical estimates based on Eq. (9) for the probe intensity amplifications and maximum ion wave electron density perturbations vs. v_d/c_s for $I^{in}_{probe}/I^{in}_{pump} = 0.17$ and 10^{-6} with $I^{in}_{pump} = 7 \times 10^{14}\mathrm{W/cm}^2$ for OMEGA crossing-beam experimental conditions.

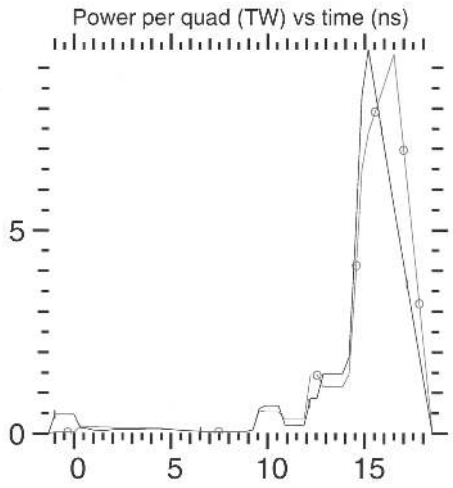

FIG. 13: Beam power versus time for the NIF ICF point design. The inner beam power peaks at 15.2ns, the outer at 16.5ns.

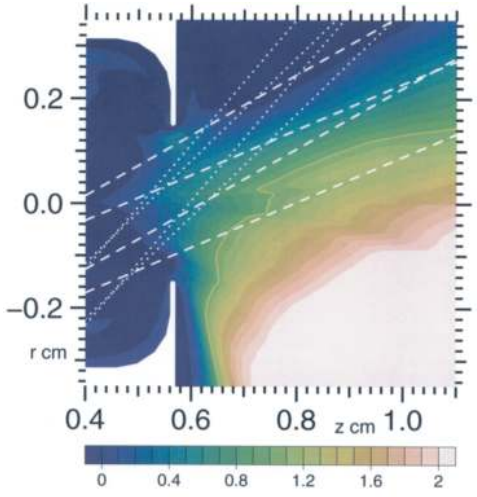

FIG. 14: Schematic of crossing beams in hohlraums at the NIF and flow Mach number for the component of the flow velocity parallel to the beat wavenumber of the crossing laser beams. The outer beams are dotted, the inner dashed.

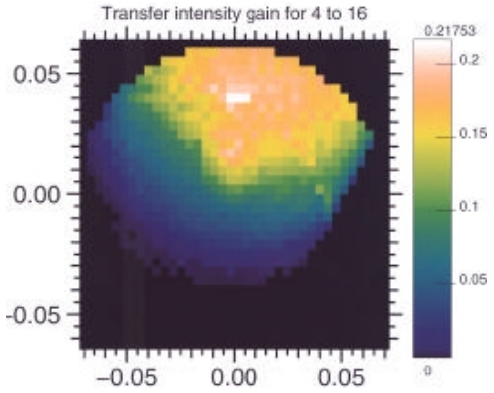

FIG. 15: Spatial gain for transfer from a 23° beam to the adjacent 44° beam as a function of position in the 23° beam cross-section.

yielded a total linear gain G as a function of position on the (elliptical) beam cross-section. Fig. 15 shows the result of this calculation for the crossing of a 23° beam with its neighbour 44° beam in azimuth. For this purpose, the results of the 3D HYDRA simulations were used to provide the required plasma conditions at 15.2ns. However, the azimuthal variation of plasma conditions in the crossing region proved not to be significant. Two-dimensional simulations would in fact have been adequate for this purpose. The figure shows that the intensity gain, $2G$ has a broad peak around 0.22.

In order to account for depletion of the inner beam power by the transfer process, the Tang [39] formula was used on a ray-by-ray basis. The amplification $\exp(2G)$ was replaced by

$$\exp(2G) \rightarrow (1+\beta)\exp(2G(1+\beta))/(1+\beta\exp(2G(1+\beta)) \quad (15)$$

Beams	0Å	1Å	2Å
$23^\circ \rightarrow 44^\circ$	10%	5%	3%
$23^\circ \rightarrow 50^\circ$	6%	3%	2%
$30^\circ \rightarrow 44^\circ$	15%	7%	2%
$30^\circ \rightarrow 50^\circ$	25%	13%	6%

TABLE I: Predicted power transfer from NIF inner to outer beams at 15.2ns in the Scale 1.1 point design, with inner beams red-shifted by 0, 1 and 2Å

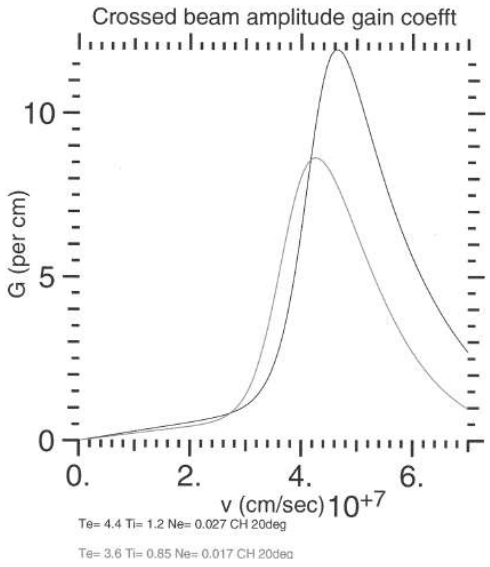

FIG. 16: Crossed beam amplitude spatial growth rate vs. transverse velocity. Beam intensities are 1.0×10^{15}W/cm^2 and 6.7×10^{15}W/cm^2. Plasma conditions are Te=4.4 (3.8) KeV, Ti=1.2 (0.85) KeV, Ne/Nc= 0.027 (0.017) in CH plasma for the upper (lower) curve.

where β is the initial ratio of outer and inner beam intensities. Integrating the result over the beam cross-section yielded a prediction for for the fractional power transfer, accounting for pump depletion, shown in Table (I). Included in this table are the corresponding results when the inner beams are red-shifted by 1Å and 2Å (at 1ω). These shifts put the ion wave farther off resonance, reducing the transfer. The NIF laser is designed to have such a capability, so this would be a possible way to mitigate the effects of power transfer.

What about the nonlinear trapping-induced frequency shifts that are the main theme of this paper? In this NIF scenario, they appear to have negligible effect. The predicted shifts are both small and less effective because the ion waves are driven off-resonance. In Figs. 17 and 18 the ion wave amplitude and trapping frequency shift are plotted as a function of transverse velocity for the conditions of Fig. 16. Kinetically derived expressions were used:

$$\frac{e\phi}{T_e} = \left| \frac{v_0 v_1}{4 v_{Te}^2} \frac{\chi_e}{1+\chi_e+\chi_i} \right| \qquad (16)$$

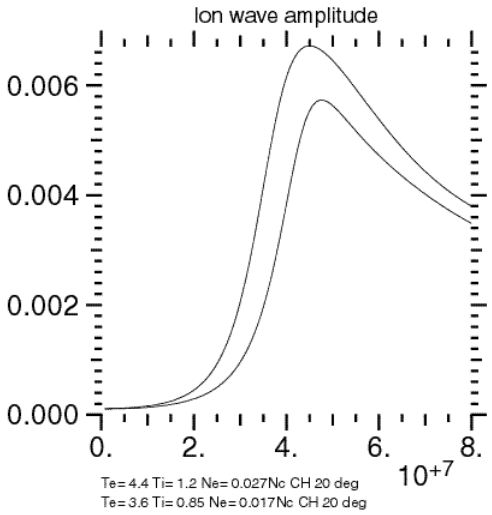

FIG. 17: Ion wave amplitude vs. transverse velocity. Beam intensities are 1.0×10^{15}W/cm^2 and 6.7×10^{15}W/cm^2. Plasma conditions are Te=4.4 (3.8) KeV, Ti=1.2 (0.85) KeV, Ne/Nc= 0.027 (0.017) in CH plasma for the solid (dashed) curve.

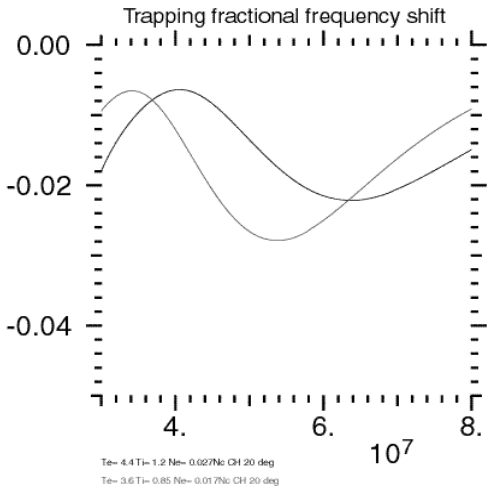

FIG. 18: Ion wave trapped particle frequency shift vs. transverse velocity. Beam intensities are 1.0×10^{15}W/cm^2 and 6.7×10^{15}W/cm^2. Plasma conditions are Te=4.4 (3.8) KeV, Ti=1.2 (0.85) KeV, Ne/Nc= 0.027 (0.017) in CH plasma for the dark (light) curve.

and

$$\frac{\delta\omega}{\omega} = -\frac{2\sqrt{2\pi}}{3\overline{\epsilon}} \sqrt{\frac{e\phi}{T_e}} \sum_i \frac{\omega_{pi}^2}{k^2} \sqrt{\frac{Z_i T_e}{M_i}} \frac{d^2 f_{Mi}}{dv^2}_{v=\omega/k} \qquad (17)$$

(the multi-species generalization of Eq. (6)). The trapping induced shifts, even if the ion waves were driven resonantly, are less than 3% of the ion acoustic frequency, which is less than the resonance width of the ion wave, making them ineffective. Most of the contribution to the shift comes from the hydrogen ions in the CH plasma, which in Eq. (17) have a relatively small weight.

Ion wave steepening and harmonic generation effects

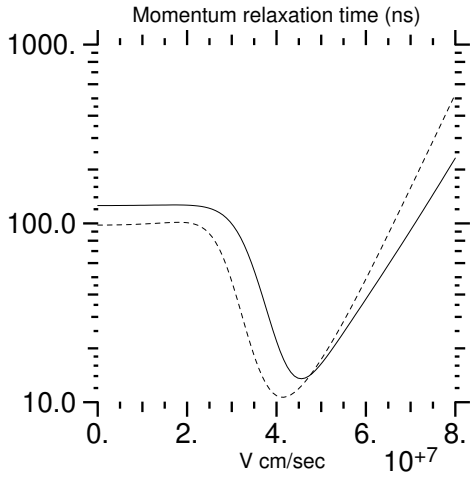

FIG. 19: The timescale for momentum deposition by light momentum $((1/\rho c_s)dp/dt)^{-1}$) is plotted versus the transverse velocity (in cm/sec). Plasma conditions are Te=4.4 (3.8) KeV, Ti=1.2 (0.85) KeV, Ne/Nc= 0.027 (0.017) in CH plasma for the solid (dashed) curve.

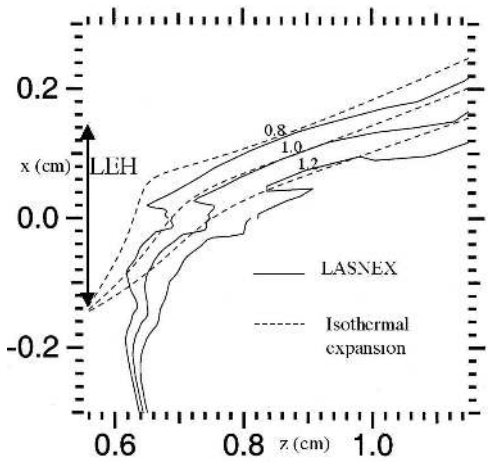

FIG. 20: Contours of the transfer component of the flow Mach number from LASNEX (at 15.2ns) and isothermal steady state expansion theory vs. axial and radial distance in front of the LEH.

scale with the square of the ion wave amplitude and so should be negligible. Likewise, two-ion-decay [5] thresholds will not be exceeded. It thus appears that ion wave nonlinearities will not mitigate the power transfer.

Another potential mechanism that could inhibit power transfer is the associated deposition of light momentum in the plasma [40], which would slow the flow and push the ion waves farther off resonance. In the Appendix, we outline the calculation of this effect. In Fig. 19 the time-scale for this process is plotted versus transverse velocity for the conditions of Fig. 16. We see that the characteristic time for the plasma flow to be slowed by the power transfer in these conditions is about 10ns on resonance and about 100ns in the hydrocode-predicted transverse flow velocities of 2-3$\times 10^7$ cm/sec. Because from Fig. 13, we see that the inner beams only remain at peak power for about 3ns, it appears that momentum deposition has insufficient time to be active.

It is not yet clear how robust these estimates are to possible changes in the NIF ICF target design. The predicted transverse velocities are at the foot of the resonance curve of Fig. 16, so relatively small changes could cause large changes in the predicted transfer. On the other hand, by analogy with gas dynamic flows through nozzles, it is plausible that the Mach number distribution outside the LEH is highly insensitive to changes in the design. As a test of this hypothesis, we computed the flow through a circular aperture of an ideal gas using the method of characteristics [41]. The flow was taken to be sonic across the aperture. The ratio of specific heats was taken to be one, the isothermal limit. Temperatures and densities scale to the conditions in the aperture, and the flow is geometrically self-similar, so there are no other free parameters in the problem. We see in Fig. 20 that the resonant Mach 1 contour from the aperture problem and from the LASNEX simulation of the NIF ICF point design are quite close, which suggests that the Mach number distribution outside the LEH is indeed generic. The most obvious discrepancies are in the H/He jet near the hohlraum axis (the isothermal model assumes a single species) and near the bottom edge of the LEH. However, these areas lie outside the crossing region.

V. SUMMARY AND DISCUSSION

In this paper we have constructed model equations describing the detuning effects of trapped-ion induced nonlinear frequency shifts in ion acoustic waves on the SBS interaction. Trapping also serves to reduce the ion Landau damping component of the total ion wave dissipation, which has an important influence on the SBS gain. The model is particularly relevant to the crossed-beam SBS interaction where the driving frequency due to the beat of the two laser beams in the plasma drift frame is well defined. Whether there is a large-amplitude ion wave present or not, the trapping induced flattening of the ion velocity distribution function shifts the ion frequency to lower values and reduces ion Landau damping. We expect that the modified velocity distribution functions can persist until collisions and thermal motion across the laser beams restore the flattened distribution functions to Maxwellian. The ion collision and ion thermal transit times across the laser beam need to be much longer than the ion bounce time due to trapping ($2\pi/k_a v_t$) and longer than the time scale for the SBS interaction to evolve to a nonlinear state, for the detuning due to trapping to have a significant influence on the SBS interaction.

The frequency shift and the reduced ion Landau damping are the central elements in our model of the trapping effects on SBS. We have solved steady-state one-dimensional equations for the amplification of the probe

electromagnetic wave (the lower frequency wave in the plasma frame of reference) and for the concomitant electron density perturbation in the ion wave. We have also included pump depletion and the effects of a linear frequency mismatch, such as would accrue from crossing beams that interact non-resonantly. Because of the nonlinear frequency shift and the neglect of the ion wave convection, there can be multiple solutions for the probe amplification and the self-consistent ion wave electron density perturbation. By means of a boundary-layer analysis, we have resolved this ambiguity and determined the physically correct solution.

We have applied our analysis of ion trapping and its effects on the SBS interaction to several examples of interest, including (i) particle simulations of a crossed-beam experiment that was conducted in the NOVA facility, (ii) a set of SBS experiments in the TRIDENT laser facility, (iii) crossed-beam experiments in the OMEGA laser facility, and (iv) proposed multiple laser-beam operation of the NIF laser facility. Our simplified theory successfully tracks the data from the BZOHAR simulations and the TRIDENT and OMEGA experiments for reasonable parameters used in the theory. The projection for NIF involves fairly complicated geometrical considerations. However, detailed post-processing of hydrocode simulations of the ICF point design indicate that the laser beams never meet the resonance condition for crossed beam transfer and ion wave nonlinearities are likely weak. Nevertheless, despite this, an analysis including pump depletion effects predicts significant energy transfer, which could be mitigated by modest shifts (1-2Å) of the inner beam laser frequency relative to the inner.

Additional research on the crossed-beam interaction is being undertaken with more sophisticated, multi-dimensional calculations including laser-beam speckle structure.

Acknowledgments

We thank Drs. R. Berger, D. DuBois, W. Kruer, M. Marinak, D. Montgomery, H. Rose, S. Pollaine and H. Vu for their valuable contributions. This work was performed under the auspices of the U.S. Department of Energy by University of California, Lawrence Livermore National Laboratory under Contract W-7405-Eng-48, and with support from LDRD 01-ERD-107.

APPENDIX A: MOMENTUM DEPOSITION BY CROSSED BEAM POWER TRANSFER

We can calculate the momentum transfer directly from the forces on the electrons and ions. The linearized Vlasov equation describing the small-amplitude electron and ion response to the beat ponderomotive potential at frequency ω and wavenumber k is

$$(-i\omega+ikv)f_{1s}-(q_s/m_s)(\phi+\delta_{es}\phi_p)ik\partial f_{0s}/\partial v = 0. \quad \text{(A1)}$$

where s is a species label. The beat ponderomotive potential $\phi_p \exp(-i\omega t + ikx) + c.c.$, where $\phi_p = -(m_e/4e)v_0 v_1^*$ acts only on the electrons (δ_{es} is a Kronecker delta function). The Poisson equation for the self-consistent electrostatic potential ϕ

$$k^2\phi = 4\pi\sum_s q_s n_{1s} = 4\pi\sum_s q_s n_{0s}\int dv f_{1s} \quad \text{(A2)}$$

closes the system. Defining the electron and ion linear susceptibilities in the usual manner with

$$\chi_s(\omega,k) = \frac{\omega_{ps}^2}{k^2}\int dv \frac{\partial f_{0s}/\partial v}{\omega - kv + i\epsilon} \quad \text{(A3)}$$

we have

$$n_{1e} = \frac{k^2\chi_e}{4\pi e}(\phi+\phi_p) \quad \text{(A4)}$$

$$n_{1i} = -\frac{k^2\chi_i}{4\pi Z_i e}\phi \quad \text{(A5)}$$

$$\phi = -\phi_p\chi_e/(1+\chi_e+\chi_i). \quad \text{(A6)}$$

Summing the forces on the particles, we obtain

$$\frac{dP}{dt} = \sum_s m_s n_{1s}^*(-\frac{q_s}{m_s}ik(\phi+\delta_{es}\phi_p)) + c.c. \quad \text{(A7)}$$

$$= \frac{k^3}{2\pi}\left(|\phi|^2\mathrm{Im}(\chi_i) + |\phi+\phi_p|^2\mathrm{Im}(\chi_e)\right) \quad \text{(A8)}$$

$$= \frac{k^3}{2\pi}|\phi_p|^2 K \quad \text{(A9)}$$

$$= \left(\frac{m_e^2}{32\pi e^2}\right)k^3 v_0^2 v_1^2 K \quad \text{(A10)}$$

$$= \left(\frac{1}{8}\right)kn_eT_e\left(\frac{v_0}{v_{Te}}\right)^2\left(\frac{v_1}{v_{Te}}\right)^2 k^2\lambda_e^2 K \quad \text{(A11)}$$

where we have defined

$$K = \mathrm{Im}(\chi_e(1+\chi_i)/(1+\chi_e+\chi_i)) \quad \text{(A12)}$$

and P is the plasma momentum density. The beam intensities are expressed in terms of the oscillatory velocities $I_{0,1} = (c/8\pi)(m\omega_0 v_{0,1}/e)^2$. Here m_e, n_e, T_e, v_{Te} and λ_e are the electron mass, density, temperature, thermal velocity and Debye length, respectively.

This result takes a more transparent form in the resonant, single ion species, quasi-neutral fluid limit in which $ZT_e \gg T_i$ and $k^2\lambda_{de}^2 \ll 1$, when $k^2\lambda_e^2 K = 2\omega/\nu_a$, where $\omega = kc_s$ and ν_a are the ion wave frequency and damping rates and $c_s^2 = ZT_e/M_i$ is the corresponding sound speed:

$$\frac{1}{\rho_m c_s}\frac{dP}{dt} = \frac{1}{16}kc_s\left(\frac{v_0}{v_{Te}}\right)^2\left(\frac{v_1}{v_{Te}}\right)^2\frac{\omega}{\nu_a} \quad \text{(A13)}$$

In this limit, on resonance, the ion wave amplitude is given by

$$\delta n/n = e\phi/T_e = (1/8)(v_0 v_1^*/v_{Te}^2)(kc_s/\nu_a)\exp(-i\omega t+ikx)+c.c., \quad \text{(A14)}$$

from which

$$(1/\rho_m c_s) dP/dt = 2\nu_a |\delta n/n|^2_{rms}. \quad \text{(A15)}$$

We see that the momentum is first transferred to ion waves by the beat ponderomotive force on the electrons. Ion wave dissipation then transfers this momentum to the bulk fluid. The characteristic time is determined by the ion wave amplitude and damping rate.

An alternative derivation considers instead the change in momentum of the light, in which case the factor K then enters through the amplitude spatial growth rate g of the forward SBS process, given by:

$$g = \frac{1}{8}\left(\frac{v_0}{c}\right)^2 \frac{k^2}{k_0} K \quad \text{(A16)}$$

[1] R. K. Kirkwood, B. B. Afeyan, W. L. Kruer, B. J. MacGowan, J. D. Moody, D. S. Montgomery, D. M. Pennington, T. L. Weiland, and S. C. Wilks, Phys. Rev. Lett. **76**, 2065 (1996).

[2] W. L. Kruer, S. C. Wilks, B. B. Afeyan, and R. K. Kirkwood, Phys. Plasmas **3**, 382 (1996).

[3] R. K. Kirkwood, B. J. MacGowan, D. S. Montgomery, B. B. Afeyan, W. L. Kruer, D. M. Pennington, S. C. Wilks, J. D. Moody, K. Wharton, C. A. Back, et al., Phys. Plasmas **4**, 1800 (1997).

[4] K. B. Wharton, C. Joshi, R. K. Kirkwood, S. H. Glenzer, K. G. Estabrook, B. B. Afeyan, B. I. Cohen, and J. D. Moody, Phys. Rev. Lett. **81**, 2248 (1998).

[5] B. I. Cohen, B. F. Lasinski, A. B. Langdon, E. A. Williams, K. B. Wharton, R. K. Kirkwood, , and K. G. Estabrook, Phys. Plasmas **5**, 3408 (1998).

[6] K. B. Wharton, R. K. Kirkwood, S. H. Glenzer, K. G. Estabrook, B. B. Afeyan, B. I. Cohen, J. D. Moody, B. J. MacGowan, and C. Joshi, Phys. Plasmas **6**, 2144 (1999).

[7] R. K. Kirkwood, J. D. Moody, A. B. Langdon, B. I. Cohen, E. A. Williams, M. R. Dorr, J. A. Hittinger, R. L. Berger, P. E. Young, L. J. Suter, et al., Phys. Rev. Lett. **89**, 215003 (2002).

[8] J. A. Paisner, E. M. Campbell, and W. J. Hogan, *National Technical Information Service Document Nos. DE95017671- DE95017673 and DE95017676-DE95017700. The Natl. Ignition Facility Project, UCRL-JC-117397 and UCRL-PROP-117093* (Copies may be obtained from the National Technical Information Service, Springfield, VA 22161, 1994).

[9] J. D. Lindl, *Inertial Confinement Fusion - The Quest for Ignition and Energy Gain Using Indirect Drive* (AIP Press, Springer Verlag, New York, 1998).

[10] D. H. Froula, L. Divol, and S. H. Glenzer, Phys. Rev. Lett. **88**, 105003 (2002).

[11] D. H. Froula, L. Divol, H. A. Baldis, R. L. Berger, D. G. Braun, B. I. Cohen, R. P. Johnson, , D. S. Montgomery, E. A. Williams, et al., Phys. Plasmas **9**, 4709 (2002).

[12] D. H. Froula, L. Divol, D. G. Braun, B. I. Cohen, G. Gregori, A. Mackinnon, E. A. Williams, S. H. Glenzer, H. A. Baldis, D. S. Montgomery, et al., Phys. Plasmas **?**, ??? (2003).

[13] S. H. Glenzer, L. M. Divol, R. L. Berger, C. Geddes, R. K. Kirkwood, J. D. Moody, E. A. Williams, and P. E. Young, Phys. Rev. Lett. **86**, 2565 (2001).

[14] L. Divol, B. I. Cohen, E. A. Williams, A. B. Langdon, B. F. Lasinski, D. H. Froula, and S. H. Glenzer, Phys. Plasmas **?**, ??? (2003).

[15] L. Divol, R. L.Berger, B. I. Cohen, E. A. Williams, A. B. Langdon, B. F. Lasinski, D. H. Froula, and S. H. Glenzer, Phys. Plasmas **?**, ??? (2003).

[16] B. I. Cohen, B. F. Lasinski, A. B. Langdon, and E. A. Williams, Phys. Plasmas **4**, 956 (1997).

[17] V. E. Zakharov and V. I. Karpman, J. Exp. Theor. Phys. **16**, 351 (1963).

[18] T. M. O'Neil, Phys. Fluids **8**, 2255 (1965).

[19] G. J. Morales and T. M. O'Neil, Phys. Rev. Lett. **28**, 417 (1972).

[20] B. I. Cohen and A. N. Kaufman, Phys. Fluids **20**, 1113 (1977).

[21] H. Ikezi, K. Schwarzeneggar, A. L. Simons, Y. Ohsawa, and T. Kamimura, Phys. Fluids **21**, 239 (1978).

[22] D. W. Forslund, J. M. Kindel, and E. L. Lindman, Phys. Fluids **18**, 1017 (1975).

[23] W. L. Kruer, Phys. Fluids **23**, 1273 (1980).

[24] W. L. Kruer and K. G. Estabrook, *Laser Plasma Interactions and Related Plasma Phenomena* (Plenum, New York, 1981), vol. 5, p. 783.

[25] B. I. Cohen and A. N. Kaufman, Phys. Fluids **21**, 404 (1978).

[26] A. A. Andreev and V. T. Tikhonchuk, Sov. Phys. JETP **68**, 1135 (1989).

[27] H. X. Vu, D. F. Dubois, and B. Bezzerides, Phys. Rev. Lett. **86**, 4306 (2001).

[28] H. A. Rose and D. Russell, Phys. Plasmas **8**, 4784 (2001).

[29] W. L. Kruer, *The Physics of Laser Plasma Interactions* (Addison-Wesley, Reading, Mass., 1988).

[30] B. I. Cohen and C. E. Max, Phys. Fluids **22**, 1115 (1979).

[31] B. I. Cohen, H. A. Baldis, R. L. Berger, K. G. Estabrook, and E. A. Williams, Phys. Plasmas **8**, 571 (2001).

[32] M. N. Rosenbluth, Phys. Rev. Lett. **29**, 565 (1972).

[33] N. K. Moncur, R. P. Johnson, R. G. Watt, and R. B. Gibson, Appl. Optics **34**, 4274 (1995).

[34] G. Zimmerman and W. Kruer, Comments Plasma Phys. Control. Fusion **2**, 85 (1975).

[35] M. M. Marinak, S. W. Haan, T. R. Dittrich, R. E. Tipton, and G. B. Zimmerman, Phys. Plasmas **4**, 1125 (1998).

[36] M. M. Marinak, G. D. Kerbel, N. A. Gentile, O. Jones, D. Munro, S. Pollaine, T. R. Dittrich, and S. W. Haan, Phys. Plasmas **8**, 2275 (2001).

[37] S. M. Pollaine, D. K. Bradley, O. L. Landen, R. J. Wallace, O. S. Jones, P. A. Amendt, L. J. Suter, and R. E. Turner, Phys. Plasmas **8**, 2357 (2001).

[38] S. W. Haan, T. Dittrich, G. Strobel, S. Hatchett, D. Hinkel, M. Marinak, D. Munro, O. Jones, S. Pollaine, and L. Suter, Fusion Science and Technology **41**, 164 (2002).

[39] C. L. Tang, J. Appl. Phys. **37**, 2945 (1966).

[40] W. L. Kruer, E. J. Valeo, and K. G. Estabrook, Phys. Rev. Lett. **35**, 1076 (1975).

[41] H. W. Liepmann and A. Roshko, *Elements of Gas Dynamics* (Dover, NY., 2002).

University of California
Lawrence Livermore National Laboratory
Technical Information Department
Livermore, CA 94551